

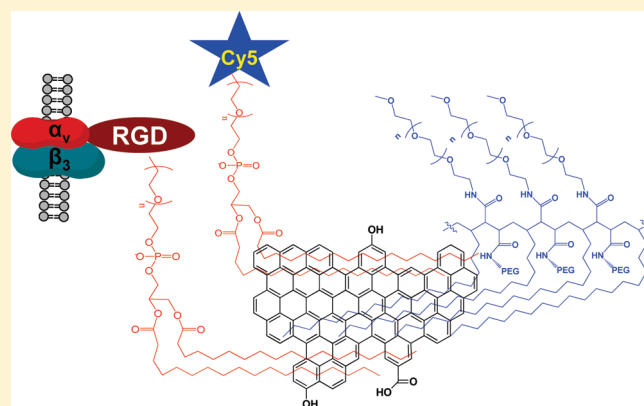
Ultrasmall Reduced Graphene Oxide with High Near-Infrared Absorbance for Photothermal Therapy

Joshua T. Robinson, Scott M. Tabakman, Yongye Liang, Hailiang Wang, Hernan Sanchez Casalongue, Daniel Vinh, and Hongjie Dai*

Department of Chemistry, Stanford University, Stanford, California 94305, United States

S Supporting Information

ABSTRACT: We developed nanosized, reduced graphene oxide (nano-rGO) sheets with high near-infrared (NIR) light absorbance and biocompatibility for potential photothermal therapy. The single-layered nano-rGO sheets were ~ 20 nm in average lateral dimension, functionalized noncovalently by amphiphilic PEGylated polymer chains to render stability in biological solutions and exhibited 6-fold higher NIR absorption than nonreduced, covalently PEGylated nano-GO. Attaching a targeting peptide bearing the Arg-Gly-Asp (RGD) motif to nano-rGO afforded selective cellular uptake in U87MG cancer cells and highly effective photoablation of cells in vitro. In the absence of any NIR irradiation, nano-rGO exhibited little toxicity in vitro at concentrations well above the doses needed for photothermal heating. This work established nano-rGO as a novel photothermal agent due to its small size, high photothermal efficiency, and low cost as compared to other NIR photothermal agents including gold nanomaterials and carbon nanotubes.



INTRODUCTION

Photothermal therapy employs photosensitizing agents taken up by cells to generate heat from light absorption,¹ leading to photoablation of the cancer cells and subsequent cell death. To avoid nonspecific heating of healthy cells, photosensitizers must show high absorption in the near-infrared (NIR)¹ and selective uptake in cancerous cells in tumors over normal cells in healthy tissues. Deep penetration and little nonspecific photothermal heating in the NIR window are due to the transparency and low absorption of light by tissues in this optical window.² Materials currently under investigation with high optical absorbance in the NIR region for photothermal therapy include gold nanoshells,³ gold nanorods,^{4–6} gold pyramids,⁷ single-walled carbon nanotubes (SWNTs),^{8–10} and multiwalled carbon nanotubes.¹¹

Graphene Oxide (GO) has recently emerged as a novel material in nanocarbon research.^{12,13} An abundant and low cost material synthesized from graphite, GO has potential use in energy,^{14,15} electronics,¹⁶ molecular sensing areas,¹⁷ and catalysis.¹⁸ A new direction for GO is in the field of biomedicine. Previous studies on nonreduced, covalently PEGylated graphene oxide (nano-GO) demonstrated effective in vitro drug delivery¹⁹ and in vivo photothermal heating²⁰ using relatively high injected doses (~ 20 mg/kg) and NIR laser powers (~ 2 W/cm²) as compared to carbon nanotubes.^{8–10} The high dose/power needed for photoablation was due to the suboptimal absorption of NIR light by nano-GO in a highly oxidized form.

Here, we developed nanosized, reduced graphene oxide (nano-rGO) sheets with noncovalent PEGylation. The nano-rGO was derived by chemically reducing covalently PEGylated nano-GO to partially restore the aromatic, conjugated character of graphene sheets, affording an increase in NIR absorbance by >6 -fold. Because of the lack of functional groups on reduced GO, a branched amphiphilic surfactant was used to coat nano-rGO noncovalently for stability and biocompatibility in biological buffer solutions. The resulting nano-rGO allowed for peptide conjugation for cancer cell targeting and selective photoablation of cancer cells at a low dose. This is the first time GO in reduced form with noncovalent PEGylation is developed for biological applications, establishing nano-rGO as a highly effective photothermal agent with comparable absorbance of NIR light to gold and carbon nanotube materials.

RESULTS AND DISCUSSION

Graphene oxide (GO) sheets (starting size ~ 5 μ m, Figure 1a,d) were synthesized using Hummers' method.²¹ To reduce the sheet size and make GO stable in buffer solutions, amine-terminated, 6-arm branched poly(ethylene glycol) (PEG) was covalently linked to the carboxylic acid groups on the graphene oxide (Figure 1b,e), while the GO solution was bath sonicated.²²

Received: February 1, 2011

Published: April 08, 2011

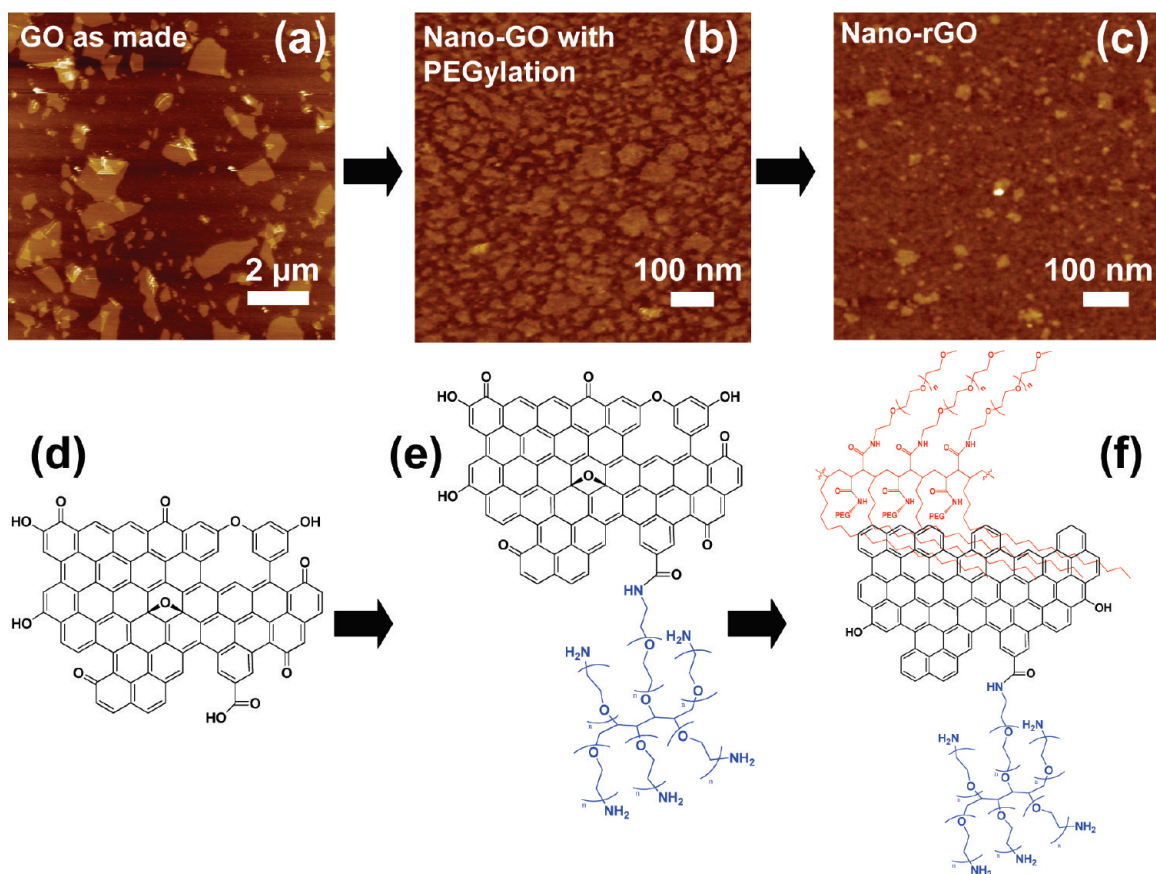


Figure 1. (a) An AFM image of as-made graphene oxide. (b) AFM of covalently PEGylated nanographene oxide (nano-GO). (c) AFM of reduced nanographene oxide (nano-rGO). All images are on a 10 nm height scale. (d)–(f) Schematic drawings of (d) as made graphene oxide, (e) nano-GO, and (f) nano-rGO illustrating the reaction steps.

Centrifugation at 22 000g removed any aggregated, multilayer sheets. We found that the step of covalent PEGylation broke the GO sheets into much smaller nano-GO pieces averaging ~ 20 nm in diameter (Figure 1b) due to the sonication process.

Next, we reduced the nano-GO sheets by adding hydrazine monohydrate into the solution and heating to 80°C for 15 min. The nano-GO solution changed color from yellow to black during the reduction step,^{23,24} indicating increased light absorption in the visible and NIR region (Figure 2a) due to recovery of conjugated π network of graphene.^{25–27} It was shown previously that similar reduction also led to increased electrical conductivity of GO.²⁸ The oxygen content in nano-GO, as measured by Auger spectroscopy, decreased from $\sim 28.5 \pm 0.8\%$ to $\sim 7.0 \pm 0.6\%$ after the reduction step. The nano-rGO aggregated in the solution after reduction due to removal of functional groups from the GO sheets. The increased hydrophobicity of the nano-rGO sheets caused aggregation even with the remaining PEG chains attached to GO through the reduction. We resuspended the nano-rGO sheets by bath sonication of the aggregates in a solution of an amphiphilic polymer,²⁹ C₁₈-PMH-mPEG₅₀₀₀ [comprised of a ~ 9 unit poly(maleamide-*alt*-1-octadecene) backbone and linear PEG chains³⁰]. Each unit in the polymer chain possessed two methoxy terminated PEG ($M_n \approx 5000$ Da) chains and one C₁₇ chain attached to the poly(maleic anhydride) backbone. The polymer coated nano-rGO (Figure 1c,f) regained stability as a homogeneous suspension in buffers and other biological solutions without aggregation even under harsh

centrifugation conditions (Figure 2a). The surfactant coating method of nano-rGO resembled the surfactant-mediated solubilization of carbon nanotubes.³¹ The lateral size of the final surfactant stabilized nano-rGO ranged from 5 to 100 nm (with a mean of ~ 18.8 nm) determined by AFM (Figure 1c) and confirmed by dynamic light scattering experiment (Figure S1).

We found that reducing nano-GO resulted in a significant ~ 6.8 fold increase in the NIR absorption at 808 nm (Figure 2b), consistent with the higher light absorption in the visible and infrared region of reduced GO previously noted.^{25–27} The increase was directly related to the degree of π conjugation in GO. Nano-GO was highly oxidized with disrupted π conjugation and therefore exhibited low electrical conductivity and low optical absorption in the visible and infrared. Chemical reduction restored part of the π conjugation and afforded increased absorption.²⁵

The high NIR absorbance of nano-rGO allowed for effective photothermal heating of solutions of low concentrations of nano-rGO (Figure 2c). At a low nano-rGO concentration of ~ 20 mg/L, rapid photothermal heating occurred upon irradiation by a low power 808 nm laser at 0.6 W/cm^2 (Figure 2c). Temperatures above the photoablation limit of 50°C (based on the Arrhenius damage integral¹) were readily reached within 5 min of irradiation. In strong contrast, under the same concentration and laser irradiation condition, a solution of nano-GO with covalent PEGylation remained below 36°C (Figure 2d). Both the nano-rGO and the nano-GO solutions exhibited a concentration-dependent

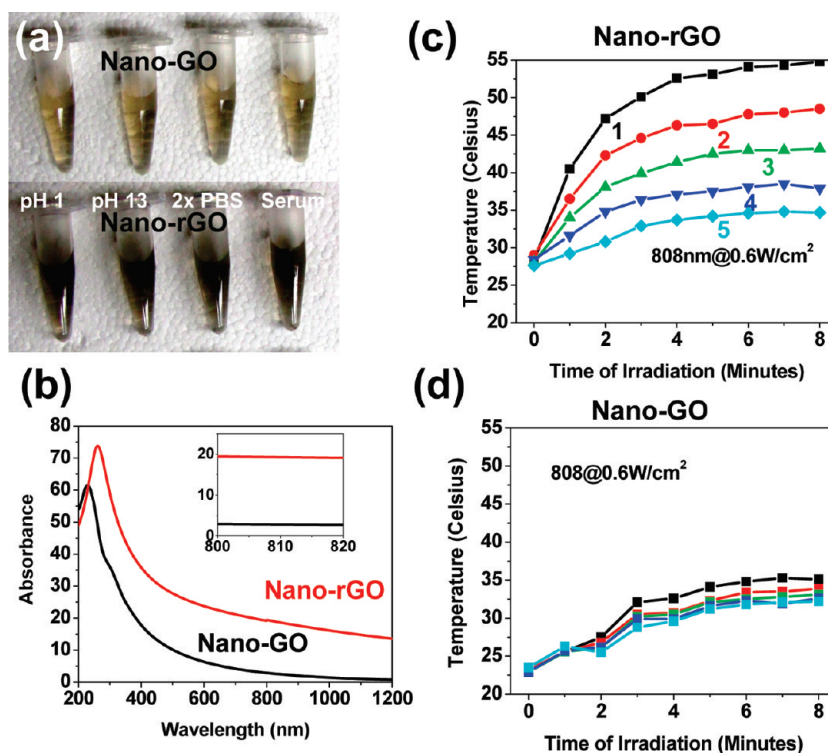


Figure 2. (a) Photographs of vials after 5 min centrifugation at 10 kg. Each vial contained 1 mL of covalently PEGylated nano-GO (top photo) or noncovalently PEGylated nano-rGO (lower photo) with the same GO mass concentration in the various solutions indicated. (b) UV–vis absorption curves of nano-GO and nano-rGO, respectively. The inset shows a zoom-in view of the curves in the 800 nm region. (c,d) Photothermal heating curves of (c) nano-rGO and (d) nano-GO solutions. Black curve (1) is 100 μ L of solution with 20 mg/L concentration of nano-rGO or -GO, red curve (2) is 10 mg/L, green curve (3) is 5 mg/L, dark blue curve (4) is 2.5 mg/L, and light blue curve (5) is water.

photothermal heating effect (from 2.5 to 20 mg/L) that increased monotonically with nano-rGO concentration (Figure 2c,d), with the former showing superior photothermal heating than the latter at all GO concentrations.

Next, fluorescent tags and Arg-Gly-Asp (RGD) or Arg-Ala-Asp (RAD)-based peptides were conjugated to the nano-rGO sheets coated with a 1:1 (by mass) mixture of C_{18} -PMH-mPEG₅₀₀₀³⁰ and DSPE-PEG₅₀₀₀-NH₂³² surfactants (see Figure 3d schematic). DSPE-PEG₅₀₀₀-NH₂ was an amphiphilic polymer with 1,2-distearoyl-3-phosphatidylethanolamine (DSPE) as the hydrophobic chain for noncovalent binding to the nano-rGO, and amine terminated poly(ethylene glycol) ($M_n \approx 5000$ Da)³² as the hydrophilic portion of the surfactant. The RGD peptide was well-known to target $\alpha_v\beta_3$ integrin receptors overexpressed on several cancer cell lines including the glioblastoma U87MG cells. The RAD peptide was used as a negative control. Following centrifuge filtration to remove any unbound surfactant molecules on nano-rGO, cyanine 5 dye (cy5) was covalently linked to the amine groups on the DSPE-PEG₅₀₀₀-NH₂ coated nano-rGO (Figure 3d). Note that a small amount of cy5 was linked to nano-rGO without using DSPE-PEG-NH₂ as a surfactant. However, the loading of cy5 on nano-rGO coated with 50% DSPE-PEG-NH₂, 50% C_{18} -PMH-mPEG was 3.3 \times the loading of cy5 on nano-rGO coated with 100% C_{18} -PMH-mPEG. Further washing steps were used to remove excess unbound cy5. Next, either RGD (+) or RAD (–) was conjugated to the remaining amine groups on DSPE-PEG₅₀₀₀-NH₂ coated nano-rGO, affording nano-rGO sheets with RGD targeting ligands (or RAD control peptide) and cy5 labels (Figure 3d).

About 5 million U87MG cells were incubated at 4 $^{\circ}$ C in a solution of nano-rGO-RAD (6.6 mg/L), nano-rGO-RGD (6.6 mg/L), or a control solution without any nano-rGO added for 1 h, collected as a cell pellet, and then washed. We chose an incubation time of 1 h and incubation temperature of 4 $^{\circ}$ C to maximize the targeting effect of nano-rGO-RGD and minimize nonspecific uptake of nano-rGO-RAD. Confocal fluorescence imaging showed that the targeted cy5 conjugate of nano-rGO-RGD gave higher signals on U87MG cells than did the non-targeted nano-rGO-RAD conjugate (Figure 3a,b). Flow cytometry confirmed a higher degree of binding of the nano-rGO-RGD conjugate to U87MG cells than the nano-rGO-RAD conjugate by ~ 3 -fold (Figure 3c). The results suggested successful conjugation of RGD peptide ligands to nano-rGO for selective cancer cell targeting and binding (Figure 3d).

We irradiated one-half of each sample of U87MG cells with an 808 nm laser for 8 min at a laser power of 15.3 W/cm² after incubations in various nano-rGO conjugates including control cells without any exposure to nano-rGO, while the remaining one-half of each U87MG cell samples were maintained as viability controls. Under irradiation, the temperature of all cell pellets increased in the first minute of irradiation and then leveled off at ~ 39 , ~ 44 , and ~ 52 $^{\circ}$ C for control cells, nano-rGO-RAD treated cells, and nano-rGO-RGD targeted cells, respectively (Figure 4a,b). After replating the cells in a 96-well plate ($n = 6$) along with the cells not exposed to 808 nm irradiation, we monitored cell viability 24 h after the photothermal treatment. U87MG cells incubated with nano-rGO-RGD and irradiated with 15 W/cm² NIR light for 8 min were completely destroyed,

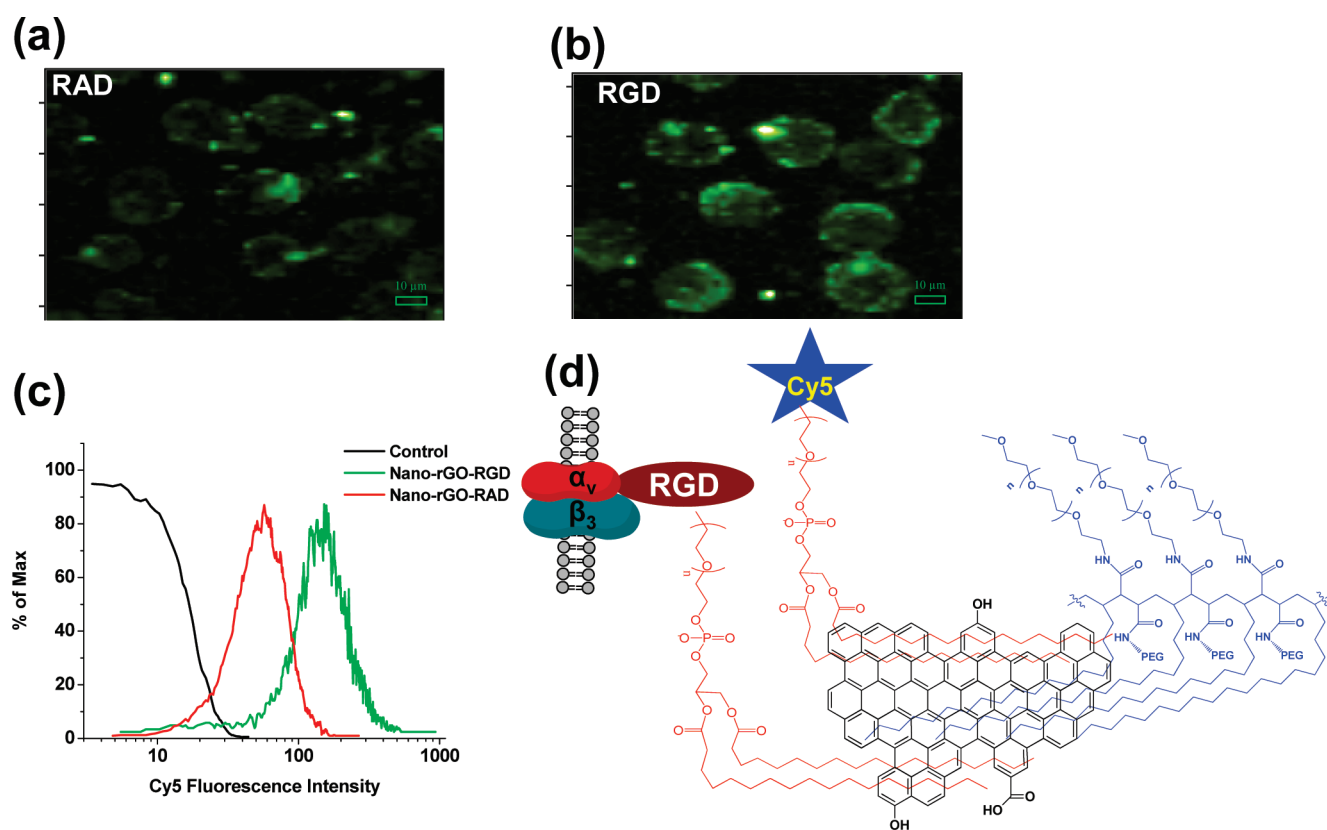


Figure 3. U87MG cell fluorescent images after incubation with (a) nano-rGO-RAD-cy5 and (b) nano-rGO-RGD-cy5. Green indicates the presence of cy5 labeled nano-rGO on the cell, and the signal is higher in (b) for nano-rGO-RGD-cy5 treated cells than in (a). (c) Flow cytometry data comparing cy5-labeled nano-rGO uptake with and without RGD targeting, which show an increase in fluorescence over untreated U87MG cells (control). The mean fluorescence intensity value of nano-rGO-RGD is 180, while the mean fluorescence intensity value of nano-rGO-RAD is 66. (d) Schematic representation of nano-rGO-RGD-cy5 interacting with $\alpha_v\beta_3$ integrin receptors on U87MG cell membrane.

while all other irradiated groups and control cells showed near 100% viability (Figure 4c). The results demonstrated successful nano-rGO targeting of U87MG cells and selective photoablation of the targeted cells.

As with any nanomaterial, toxicity is a concern. To this end, we examined the biocompatibility of nano-rGO with several cell lines and compared it to covalently PEGylated nano-GO (Figure 5a–c). Nano-GO and nano-rGO appeared to show similar levels of toxicity despite the covalent PEGylation of nano-GO versus noncovalent PEGylation of nano-rGO. The half maximal inhibitory concentration (IC_{50}) of nano-rGO was found to be ~ 80 mg/L, while nano-GO has an IC_{50} of ~ 99 mg/L for the human breast cancer line MCF-7. Note that previously it was found that as-made GO without any PEGylation decreased the viability of A459 cells (a human lung carcinoma cell line) at 100–200 mg/L.³³ In our experiments, the concentration of nano-rGO used for incubating U87MG cells was ~ 6.6 mg/L, an order of magnitude lower than the IC_{50} of nano-rGO. Therefore, we expect that the concentrations of nano-rGO in the cellular environment and in blood for in vitro and in vivo experiments will be well below the IC_{50} of this material.

We also found that nano-rGO sheets were capable of loading doxorubicin noncovalently (Figure S2) via π -stacking in a manner similar to previous results of nano-GO loading hydrophobic chemotherapy drugs such as camptothecin and doxorubicin.^{19,22} Hence, nano-rGO could be used to combine photothermal and chemotherapy in a synergistic manner to

decrease the dose needed for both the photothermal agent (i.e., nano-rGO) and the drug.³⁴ The small size of the nano-rGO (Figure 1c) should facilitate high tumor uptake in vivo through the enhanced permeability and retention (EPR) effect.³⁵ These aspects warrant systematic future research of nano-rGO for in vivo cancer treatment.

As compared to other nanomaterials with NIR light absorption, on a per mass basis, nano-rGO exhibits a higher absorption of NIR light than gold nanorods that have been demonstrated as effective photothermal therapy agents.⁴ The mass extinction coefficient for nano-rGO at 808 nm is 24.6 L/(g·cm), nearly twice that of gold nanorods [13.89 L/(g·cm)].¹⁰ As compared to single-walled carbon nanotubes [46.5 L/(g·cm)],¹⁰ nano-rGO exhibits a 47% lower mass extinction coefficient. Nevertheless, the low cost of nano-rGO relative to gold and SWNTs makes it attractive as a possible photothermal agent at large scales.

CONCLUSION

We have developed biocompatible, reduced graphene oxide sheets for potential photothermal therapy. The average size of nano-rGO sheets was small, ~ 20 nm afforded by sonication during covalent PEGylation. Chemical reduction of nano-GO afforded >6 -fold increase in the NIR absorbance of the resulting nano-rGO, making it a highly NIR absorbing photothermal agent comparable to carbon nanotubes and gold-based nanomaterials. We demonstrated functionalization of nano-rGO by targeting

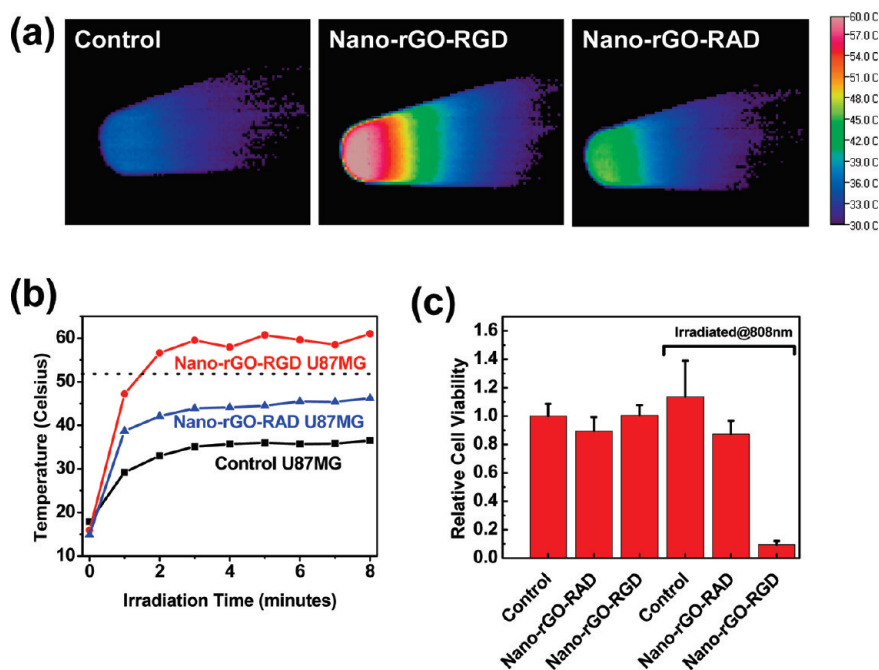


Figure 4. (a) Thermal images of vials containing pellets of control nontreated U87MG cells, cells treated by nano-rGO-RGD, and cells treated by nano-rGO-RAD, respectively, after 8 min of irradiation with an 808 nm laser at a power of 15.3 W/cm². (b) Cell pellet temperature versus time during irradiation and (c) cell viability 24 h post irradiation.

ligands for selective cancer cell uptake and photothermal ablation in vitro. This work shall lead to systematic in vivo investigations of nano-rGO for photothermal treatment of tumor models in mice using low doses of nano-rGO at low laser powers.

EXPERIMENTAL SECTION

Nano-GO Synthesis. Graphene oxide (GO) was synthesized using Hummers' method²¹ at a gram scale from graphitic flakes (Superior Graphite Co.). Following synthesis, 10 mL of GO, at a concentration of approximately 1000 mg/L, had 1.2 g of sodium hydroxide added (J.T. Baker Inc.). This solution was sonicated for 3 h, and then concentrated hydrochloric acid (12.1 N, Fisher Scientific) was added until the pH dropped to 1. The solution was then washed three times with water and brought to a concentration of 1000 mg/L. Six-armed branched poly(ethylene glycol) (Laysan Bio, Inc.) with amine termination (6PEG-NH₂) was added to the solution at 2000 mg/L and sonicated for 5 min. *N*-(3-Dimethylaminopropyl-*N'*-ethylcarbodiimide) hydrochloride (EDC, Sigma-Aldrich) was added to the solution (0.76 mmol) followed by sonication for an additional 1 h. The GO solution was then centrifuged at 22 000g for 6 h in double phosphate buffer saline (PBS, 0.8% NaCl, 0.02% KCl, and 0.02 M PO₄) to remove any aggregates or multilayered GO sheets (confirmed by AFM). The supernatant was collected after centrifugation and washed eight times and filtered each time through a 100 kDa MWCO centrifuge filter (Millipore) at 4000g.

Nano-rGO Synthesis. Reduced nanographene oxide was synthesized in a manner similar to that of graphene oxide. However, before centrifugation at 22 000g, 0.05% v/v of hydrazine monohydrate (Fluka Inc.) was added, and the solution is heated to 80 °C for 15 min (at which point the solution darkened from a translucent yellow to an opaque black color and visible aggregates began to form). To resuspend the solution, 1000 mg/L of the polymer C₁₈-PMH-mPEG₅₀₀₀³⁰ was added, and another 1 h sonication took place. Centrifugation was then done at 22 000g to remove any aggregates or multilayered nano-rGO sheets. The supernatant was collected after centrifugation and washed eight times

with 100 kDa MWCO Millipore centrifuge filter at 4000g. C₁₈-PMH-mPEG₅₀₀₀ was synthesized using methoxy poly(ethylene glycol)-amine (5 kDa MW, mPEG-NH₂, Laysan Bio, Inc.), EDC, and polymaleic anhydride-*alt*-1-octadecene (3.2 kDa MW). The polymaleic anhydride-*alt*-1-octadecene was synthesized by 2,2'-azobisisobutyronitrile (AIBN) initiated free radical polymerization of maleic anhydride and octadecene.³⁶ The monomers and initiator ratio were controlled to produce poly(maleic anhydride-*alt*-1-octadecene) with an average molecular weight of 3.2 kDa.

Spectroscopic Characterization. The absorbance spectra of nano-GO and nano-rGO were taken using a Varian Cary 6000i with a 1 cm quartz cuvette. The concentration was determined using a mass extinction coefficient of 61.5 L/g·cm at 230 nm for nano-GO and 73.8 L/g·cm at 265 nm for nano-rGO. Stability of the nano-GO and nano-rGO was tested for 1 mL at a concentration of 10 mg/L at pH 1, pH 13, in double PBS described above, and in 50% fetal bovine serum (FBS). Each solution was centrifuged at 10 000g for 5 min.

Graphene oxide (before and after PEGylation) and nano-rGO sheets were imaged with atomic force microscopy (AFM) on a silicon substrate. Auger spectra were taken with a PHI 700TM scanning auger nanoprobe. The acceleration voltage was 10 kV, and the emission current was 10 nA.

Peptide and Cy5 Conjugation to nano-rGO. Nano-rGO in a 1:1 mixture of DSPE-PEG₅₀₀₀-NH₂ (Laysan Bio Inc.) and C₁₈-PMH-mPEG₅₀₀₀ was repeated filtered through 100 kDa MWCO centrifugal filter units (Amicon Ultra) to remove free DSPE-PEG₅₀₀₀-NH₂. The solution was resuspended in 1 mL of 0.1 M phosphate buffered saline (PBS). Stock solutions of sulfo-succinimidyl-4-(*N*-maleimido-methyl)cyclohexane-1-carboxylate (sulfo-SMCC, Pierce) and cyanine dye 5, mono-NHS ester (cy5-NHS, GE Lifesciences) were prepared in a minimal volume of dry DMSO and immediately added to 1 mL of the filtered nano-rGO solution at final concentrations of approximately 300 μM sulfo-SMCC, 50 μM cy5-NHS, and 66 mg/L nano-rGO. The reaction proceeded for 2 h at room temperature, and remaining cross-linker and dye were removed by repeated filtration and resuspension of the solution through 100 kDa MWCO centrifugal units. The solution was resuspended into two 500 μL aliquots in PBS.

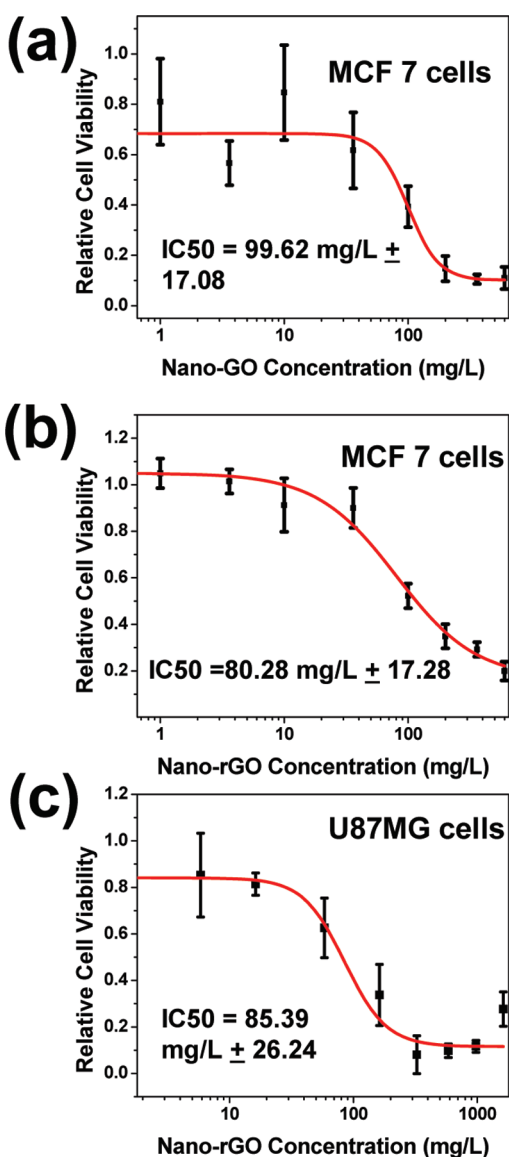


Figure 5. Cellular viability data based on MTS colorimetric assay for (a) MCF-7 cells incubated for 48 h with nano-GO, (b) MCF-7 cells incubated for 48 h with nano-rGO, and (c) U87MG cells incubated for 48 h with nano-rGO.

Stock solutions of cyclo(RGDFC) and cyclo(RADFC) peptides (RGD and RAD, respectively, Peptides International) were prepared at 10 mM in PBS. A 0.1 M stock solution of tris(2-carboxyethyl)phosphine hydrochloride (TCEP, Sigma-Aldrich) was prepared in PBS and neutralized to pH 7 with 1 M sodium hydroxide. 75 nmol (7.5 μ L) of RGD and RAD was added to separate vials, each containing 100 μ L of 20 mM TCEP in PBS to reduce any naturally occurring disulfide bonds. The peptide and TCEP mixtures were each added to the 500 μ L aliquots of nano-rGO-cy5 solution, and coupling of the peptide was allowed to proceed for 48 h at 4 $^{\circ}$ C. The reaction mixtures were then repeatedly filtered again through 100 kDa MWCO centrifugal filter units to remove remaining free peptide and other reagents. Finally, the nano-rGO-RGD and nano-rGO-RAD solutions were resuspended in 250 μ L.

Cell Incubation. U87MG human glioblastoma cells (ATCC: HTB-14) were cultured in DMEM media containing 1 g/L glucose, 10% fetal bovine serum (FBS), and penicillin/streptomycin. For staining with nano-rGO-peptide conjugates, the cells were released (0.25%

trypsin-EDTA, Gibco), resuspended, and washed by centrifugation at 400g into DMEM media containing 10% FBS. Three aliquots of approximately 5 million cells were resuspended in 200 μ L of media. To one of these aliquots was added nano-rGO-RGD at 1:10 dilution (6.6 mg/L); nano-rGO-RAD was added at the same dilution to another aliquot. The remaining aliquot was kept as an unstained treated control. The cells were incubated with nano-rGO at 4 $^{\circ}$ C for 1 h followed by three washes by centrifugation and resuspension to remove media and any free nano-rGO. Finally, 10 μ L of each aliquot of cells (control, nano-rGO-RGD, and nano-rGO-RAD) was removed for confocal fluorescence imaging, and the remaining cells were resuspended to 100 μ L and split into two 50 μ L volumes, which were again centrifuged to form a pellet at 400g.

Photothermal Irradiation. After 1 h of incubation at 4 $^{\circ}$ C with nano-rGO-RGD, nano-rGO-RAD, or control, the vials containing cell pellets were stored in ice until irradiation. The cell pellets were irradiated for 8 min in a 1.5 mL vial with an 808 nm laser at a power of 15.3 W/cm² (0.3 cm² laser area). The source of irradiation was a 20W 808 nm diode laser (RPMC lasers). Thermal images were taken every minute with a MikroShot camera (Mikron). Immediately after heating, cells were plated in a 96-well plate with 100 μ L of media. After 24 h of incubation at 37 $^{\circ}$ C, cell viability was determined by MTS assay using a CellTiter96 kit (Promega).

Toxicity Assessment. Nano-rGO and nano-GO toxicity was determined by MTS assay using a CellTiter96 kit on U87MG and MCF7 human epithelial breast cancer cells (AATC: HTB-22). \sim 4000 cells/well were plated in a 96-well plate with 100 μ L of media at various concentrations of nano-GO and nano-rGO solutions. Incubation time was 48 h. Nano-rGO and nano-GO solutions were removed from the well plates immediately prior to addition of colorimetric indicator to prevent any interference in the absorbance readings.

■ ASSOCIATED CONTENT

S Supporting Information. Further characterization of the size and toxicity of nano-rGO. This material is available free of charge via the Internet at <http://pubs.acs.org>.

■ AUTHOR INFORMATION

Corresponding Author

hdai@stanford.edu

■ ACKNOWLEDGMENT

This work was supported by Ensysce Biosciences, CCNE-TR at Stanford University, and NIH-NCI RO1 CA135109-02.

■ REFERENCES

- (1) Splinter, R.; Hooper, B. A. *An Introduction to Biomedical Optics*; Taylor & Francis: New York, 2007; pp 220–232.
- (2) Welsher, K.; Liu, Z.; Sherlock, S. P.; Robinson, J. T.; Chen, Z.; Daranciang, D.; Dai, H. *Nat. Nanotechnol.* **2009**, *4*, 773.
- (3) Hirsch, L. R.; Stafford, R. J.; Bankson, J. A.; Sershen, S. R.; Rivera, B.; Price, R. E.; Hazle, J. D.; Halas, N. J.; West, J. L. *Proc. Natl. Acad. Sci. U.S.A.* **2003**, *100*, 13549–13555.
- (4) von Maltzahn, G.; Park, J.-H.; Agrawal, A.; Bandaru, N. K.; Das, S. K.; Sailor, M. J.; Bhatia, S. N. *Cancer Res.* **2009**, *69*, 3892–3900.
- (5) Dickerson, E. B.; Dreaden, E. C.; Huang, X.; El-Sayed, I. H.; Chu, H.; Pushpanketh, S.; McDonald, J. F.; El-Sayed, M. A. *Cancer Lett.* **2008**, *269*, 57.
- (6) Tong, L.; Wei, Q.; Wei, A.; Cheng, J.-X. *Photochem. Photobiol.* **2009**, *85*, 21.

- (7) Hasan, W.; Stender, C. L.; Lee, M. H.; Nehl, C. L.; Lee, J.; Odom, T. W. *Nano Lett.* **2009**, *9*, 1555.
- (8) Kam, N. W. S.; O'Connell, M.; Wisdom, J. A.; Dai, H. *Proc. Natl. Acad. Sci. U.S.A.* **2005**, *102*, 11600–11605.
- (9) Zhou, F.; Xing, D.; Ou, Z.; Wu, B.; Resasco, D. E.; Chen, W. R. *J. Biomed. Opt.* **2009**, *14*, 021009.
- (10) Robinson, J.; Welscher, K.; Tabakman, S.; Sherlock, S.; Wang, H.; Luong, R.; Dai, H. *Nano Res.* **2010**, *3*, 779.
- (11) Ghosh, S.; Dutta, S.; Gomes, E.; Carroll, D.; D'Agostino, R.; Olson, J.; Guthold, M.; Gmeiner, W. H. *ACS Nano* **2009**, *3*, 2667.
- (12) Compton, O. C.; Nguyen, S. T. *Small* **2010**, *6*, 711.
- (13) Yang, X.; Zhang, X.; Liu, Z.; Ma, Y.; Huang, Y.; Chen, Y. *J. Phys. Chem. C* **2008**, *112*, 17554.
- (14) Wang, H.; Cui, L.-F.; Yang, Y.; Sanchez Casalongue, H.; Robinson, J. T.; Liang, Y.; Cui, Y.; Dai, H. *J. Am. Chem. Soc.* **2010**, *132*, 13978.
- (15) Wang, H.; Casalongue, H. S.; Liang, Y.; Dai, H. *J. Am. Chem. Soc.* **2010**, *132*, 7472.
- (16) Wang, H.; Wang, X.; Li, X.; Dai, H. *Nano Res.* **2009**, *2*, 336.
- (17) Robinson, J. T.; Perkins, F. K.; Snow, E. S.; Wei, Z.; Sheehan, P. E. *Nano Lett.* **2008**, *8*, 3137.
- (18) Liang, Y.; Wang, H.; Sanchez Casalongue, H.; Chen, Z.; Dai, H. *Nano Res.* **2010**, *3*, 701.
- (19) Liu, Z.; Robinson, J. T.; Sun, X.; Dai, H. *J. Am. Chem. Soc.* **2008**, *130*, 10876.
- (20) Yang, K.; Zhang, S.; Zhang, G.; Sun, X.; Lee, S.-T.; Liu, Z. *Nano Lett.* **2010**, *10*, 3318–3323.
- (21) Hummers, W. S.; Offeman, R. E. *J. Am. Chem. Soc.* **1958**, *80*, 1339.
- (22) Sun, X.; Liu, Z.; Welscher, K.; Robinson, J.; Goodwin, A.; Zaric, S.; Dai, H. *Nano Res.* **2008**, *1*, 203.
- (23) Kim, S. R.; Parvez, M. K.; Chhowalla, M. *Chem. Phys. Lett.* **2009**, *483*, 124.
- (24) Liu, Y.; Huang, L.; Ji, L. C.; Wang, T.; Xie, Y. Q.; Liu, F.; Liu, A. Y. *Vacuum Electron Sources Conference and Nanocarbon (IVESC)*, 2010 8th International, 14–16 Oct. 2010; p 463.
- (25) Kim, J.; Kim, F.; Huang, J. *Mater. Today* **2010**, *13*, 28.
- (26) Acik, M.; Lee, G.; Mattevi, C.; Chhowalla, M.; Cho, K.; Chabal, Y. J. *Nat. Mater.* **2010**, *9*, 840.
- (27) Li, D.; Muller, M. B.; Gilje, S.; Kaner, R. B.; Wallace, G. G. *Nat. Nanotechnol.* **2008**, *3*, 101.
- (28) Wang, H.; Robinson, J. T.; Li, X.; Dai, H. *J. Am. Chem. Soc.* **2009**, *131*, 9910.
- (29) Qi, X.; Pu, K.-Y.; Li, H.; Zhou, X.; Wu, S.; Fan, Q.-L.; Liu, B.; Boey, F.; Huang, W.; Zhang, H. *Angew. Chem., Int. Ed.* **2010**, *49*, 9426.
- (30) Prencipe, G.; Tabakman, S. M.; Welscher, K.; Liu, Z.; Goodwin, A. P.; Zhang, L.; Henry, J.; Dai, H. *J. Am. Chem. Soc.* **2009**, *131*, 4783.
- (31) Liu, Z.; Tabakman, S.; Welscher, K.; Dai, H. *Nano Res.* **2009**, *2*, 85.
- (32) Liu, Z.; Tabakman, S. M.; Chen, Z.; Dai, H. *Nat. Protoc.* **2009**, *4*, 1372.
- (33) Chang, Y.; Yang, S.-T.; Liu, J.-H.; Dong, E.; Wang, Y.; Cao, A.; Liu, Y.; Wang, H. *Toxicol. Lett.* **2011**, *200*, 201.
- (34) Park, H.; Yang, J.; Lee, J.; Haam, S.; Choi, I.-H.; Yoo, K.-H. *ACS Nano* **2009**, *3*, 2919.
- (35) Whitesides, G. M. *Nat. Biotechnol.* **2003**, *21*, 1161.
- (36) Davies, M. C.; Dawkins, J. V.; Hourston, D. J.; Meehan, E. *Polymer* **2002**, *43*, 4311.